

Blocks World Revisited: The Effect of Self-Occlusion on Classification by Convolutional Neural Networks

Markus D. Solbach
York University
solbach@eecs.yorku.ca

John K. Tsotsos
York University
tsotsos@eecs.yorku.ca

Abstract

Despite the recent successes in computer vision, there remain new avenues to explore. In this work, we propose a new dataset to investigate the effect of self-occlusion on deep neural networks. With TEOS (The Effect of Self-Occlusion), we propose a 3D blocks world dataset that focuses on the geometric shape of 3D objects and their omnipresent challenge of self-occlusion. We designed TEOS to investigate the role of self-occlusion in the context of object classification. Even though remarkable progress has been seen in object classification, self-occlusion is a challenge. In the real-world, self-occlusion of 3D objects still presents significant challenges for deep learning approaches. However, humans deal with this by deploying complex strategies, for instance, by changing the viewpoint or manipulating the scene to gather necessary information. With TEOS, we present a dataset of two difficulty levels (L_1 and L_2), containing 36 and 12 objects, respectively. We provide 738 uniformly sampled views of each object, their mask, object and camera position, orientation, amount of self-occlusion, as well as the CAD model of each object. We present baseline evaluations with five well-known classification deep neural networks and show that TEOS pose a significant challenge for all of them. The dataset, as well as the pre-trained models, are made publicly available for the scientific community under <https://data.nvision.eecs.yorku.ca/TEOS/>.

1. Introduction

Over most of the last decade, computer vision was pushed by efforts put into deep learning. The exact advent of this deep learning dominated era is often dated to the ImageNet challenge ([Russakovsky et al., 2015]) in 2012. Since then, the performance of models on various tasks has been improving at unparalleled speed; for instance, image classification on the ImageNet dataset surpassed the reported human-level performance in 2015

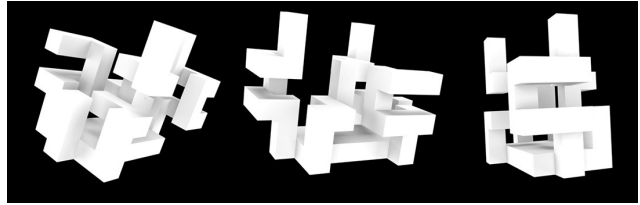


Figure 1. Example of the proposed objects from three different viewpoints.

([He et al., 2015]). Two of the enablers for the recent successes are faster computers, specifically graphic processors, and the availability of large scale and often well-curated data sets to learn from.

The deep learning paradigm is omnipresent, and, with it, the need for data with specific statistics to work in certain domains. [Kuznetsova et al., 2020] goes as far as saying that "Data is playing an especially critical role in enabling computers to interpret images as compositions of objects, an achievement that humans can do effortlessly while it has been elusive for machines so far."

Many domains exist in which one would like machines to perform visual tasks ([Carroll and Others, 1993]). One of these is object classification, which is defined as whether a particular item is present in the stimulus ([Tsotsos et al., 2005]).

Object classification is an essential capability of humans, as well as for any robotic system whose goal is to be a real-world assistant; in a factory, hospital, or at home, just to name a few. Even though very successful in many domains, deep learning methods are challenged with occlusion ([Koporec and Pers, 2019]), which is inevitable in real-world scenarios. Here, we go a step further and show that deep learning methods are also challenged with the self-occlusion of objects, hence not generalizing to objects' 3D structure.

The problem of understanding the 3D structure from a 2D description, for instance, a line drawing, was first put forward independently by [Huffman, 1971] and

[Clowes, 1971], and they both showed that the necessary critical condition for a line drawing to represent an actual arrangement of polyhedral objects was labelability.

As the human brain is very efficient at reconstructing a scene’s 3D structure from a single image with no texture, colour or shading, efforts have been concentrated on computational complexity issues; one might think an efficient solution exists (e.g. polynomial-time). [Kirosis and Papadimitriou, 1988], however, proved that this problem is NP-Complete, also for simple cases like trihedral, solid scenes. To further research in this field, [Parodi et al., 1998] proposed a method to generate random instances of line drawings with useful distribution to investigate questions related to complexity of understanding images of polyhedral scenes. More recently, [Solbach et al., 2018] provided a 3D extension with controllable camera parameters and two different light settings. It is designed to enable research on how a program could parse a scene if it had multiple and definable viewpoints to consider. An example of a polyhedral scene from [Solbach et al., 2018] is shown from three different viewpoints in Figure 2.

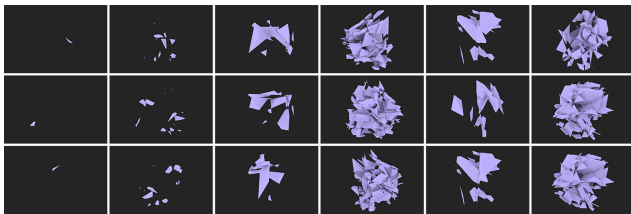


Figure 2. Six polyhedral scenes from three different viewpoints with increasing complexity ([Solbach et al., 2018]).

With the increasing successes, contemporary computer vision approaches show a healthy trend away from artificial problems and provide solutions to real-world problems, already deployed in many domains ([Andreopoulos and Tsotsos, 2013]), for example, optical character recognition, industrial inspection systems, medical imaging, and biometrics. However, at the same time, a disparagement of artificial domains can be seen ([Slaney and Thiébaux, 2001]). At the very least, these domains can support meaningful systematic experiments. Here we revisit one such artificial domain; the Blocks World.

In visual perception, the basic physical and geometric constraints of our world play a crucial role. This idea goes back at least to Helmholtz and his argument for *unconscious inference*.

This theme of visual perception can be traced back to the early years of the discipline of computer vision. Larry Roberts argued that “the perception of solid objects is a process which can be based on the properties of

three-dimensional transformations and the laws of nature” ([Roberts, 1965]). Roberts’ popular Blocks World was an early attempt to build a system for complete scene understanding for a closed artificial world of textureless polyhedral shapes by using a generic library of polyhedral block shapes. This toy domain that has remained as a staple of the AI literature for over 30 years but has fallen into disrepute since then. This is due to a superficial understanding of it, leading to insufficient experimental methodology, and therefore, failing to extract useful results from it ([Slaney and Thiébaux, 2001]).

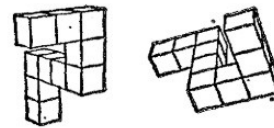


Figure 3. Example of the objects by [Shepard and Metzler, 1971] which are used as an inspiration.

In this paper, we present *TEOS: The Effect of Self-Occlusion*. *TEOS* is a Blocks World based set of objects with known complexity, controlled viewpoints, with a known level of self-occlusion and 3D models. *TEOS* shares similarities in appearance with the so-called Shepard and Metzler Objects ([Shepard and Metzler, 1971]), which are widely used in the literature for mental rotation tasks. See Figure 3 for an illustration of two such objects. Similarities are for instance, the strict ninety-degree angle of elements making up an object, the use of only cuboids, the use of mainly one primitive (except for the base plate).

However, with *TEOS*, we present a set of objects that go beyond the Shepard and Metzler objects. Specifically, our objects have a known complexity, share a common coordinate system, and empirical results have shown that they are challenging for visual tasks using state-of-the-art classification algorithms.

Our contributions are an investigation of the effect of self-occlusion for object classification. To accomplish this, we provide a novel set of objects, a carefully created dataset, including an in-depth explanation of the objects and generated data with a focus on self-occlusion and a baseline evaluation with state-of-the-art classification algorithms.

The remainder of the paper is structured as follows. First, we will explain in detail the objects we have created for *TEOS*. We then continue by giving an overview of related work, describing the data acquisition, presenting our self-occlusion measure, evaluating the dataset against state-of-the-art classification algorithms, and finally finishing with our conclusions and future directions.

2. Related Work

To the best of our knowledge, self-occlusion has not attracted much attention in the literature. However, occlusion caused by other objects has. In addition to several datasets, a number of approaches were introduced to deal with occlusion.

2.1. Occlusion Datasets

A burden of deep learning is its need for vast mounts of training data. Even though occlusion and its effect on vision tasks has been addressed for some time ([Hsiao et al., 2010, Ouyang and Wang, 2012, Brachmann et al., 2014, Hsiao and Hebert, 2014]), datasets created are usually too small to be used to train successful deep learning models. Furthermore, to our knowledge, datasets, if considering occlusion, mostly introduce various levels of clutter but lack to define occlusion in a generic way. For instance, the CMU Kitchen Occlusion dataset (CMU_KO8) by [Hsiao and Hebert, 2014] consists of 1,600 images of eight kitchen objects, such as backing pan, scissors, etc., which only yields 200 examples per class. The dataset has explicitly been designed to challenge object recognition algorithms with strong viewpoint and illumination changes, occlusions and clutter. Besides a novel dataset, an occlusion reasoning module is also proposed (further details in Section 2.2).

With the *ICCV 2015 Occluded Object Challenge* ([Hinterstoisser et al., 2013, Brachmann et al., 2014]), a dataset with eight objects positioned in a realistic setting of heavy occlusion is presented. The objects can be described as being of different domains, ranging from animals, over office supplies, to kitchenware. However, neither a definition of occlusion nor a metric is given. Figure 4 shows an example image of the dataset.



Figure 4. A scene with different objects under occlusion taken from the *ICCV 2015 Occluded Object Challenge*.

The majority of occlusion datasets, however, deal with the occlusion of pedestrians. Specifically, in the con-

text of autonomous driving, detecting pedestrians, even if occluded, is crucial to detect potential collisions. It is argued that most existing datasets are not designed for evaluating occlusion. For instance, the Caltech dataset ([Dollár et al., 2012]) only contains 105 out of 4250 images with occluded pedestrians. The CUHK Occlusion Dataset ([Ouyang and Wang, 2012]) is specifically designed as a pedestrian dataset with occlusion. The authors selected images from popular pedestrian datasets and recorded images from surveillance cameras and filtered them mainly for occluded pedestrians. The dataset contains 1,063 images with binary classification to indicate whether the pedestrian is occluded or not.

2.2. Occlusion Reasoning

Reasoning about occlusion has been used in many areas, from object recognition to tracking and segmentation. Reported in ([Hsiao and Hebert, 2014], the literature is extensive, but there has been comparatively little work on modelling occlusions from different viewpoints and using 3D information until recently. Further, occlusion reasoning is broadly classified into five categories; inconsistent object statistics, multiple images, part-based models, 3D reasoning, and convolutional neural networks.

The first category includes classical approaches, which use inconsistent object statistics to reason about potential occlusion. In general, occlusions are modelled as regions that are inconsistent with object statistics. For instance, [Meger et al., 2011] use inconsistencies in 3D sensor data to classify occlusions. [Girshick et al., 2011] introduce an occluder part in their grammar model when all parts cannot be placed. [Wang et al., 2009] use a scoring metric based on individual HOG filter cells. [Hsiao and Hebert, 2014] incorporate occlusion reasoning in object detection in a two-stage manner. First, in a bottom-up stage, occluded regions are hypothesized from image data. Second, a top-down stage is used that relies on prior knowledge to score the candidates' occlusion plausibility. Extensive evaluation on single, as well as multiple views show that incorporating occlusion reasoning yields significant improvement in recognizing texture-less objects under severe occlusions.

The use of multiple images characterizes the second category. For these approaches, a sequence of consecutive images is necessary to disambiguate the object from occluders. For instance, [Ess et al., 2009] detects the objects and extrapolates the state of occluded objects using an Extended Kalman Filter. Reliable tracklets that are used in a temporal sliding window fashion are generated to disambiguate occluded objects in [Xing et al., 2009].

One of the largest categories are approaches using part-based models. A challenge of global object templates is occlusion as their performance degrades with its presence significantly. A popular solution to this problem is to sepa-

rate the object into a set of parts and detect parts individually. This approach generally yields more robust detections towards occlusion. For example, [Shu et al., 2012] analyze the contribution of each part using a linear SVM and train the classifier to use unoccluded parts to maximize the probability of detection. [Wu and Nevatia, 2009] go a step further and use multiple part detectors to maximize the joint likelihood. Binary classification of parts is introduced by [Vedaldi and Zisserman, 2009]. They decompose the HOG descriptor into small blocks that selectively switch between an object and an occlusion descriptor.

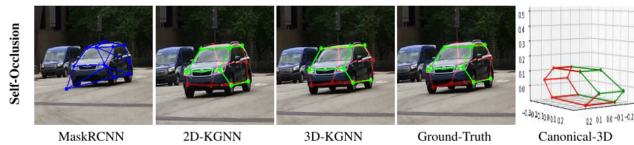


Figure 5. The effect of occlusion reasoning used in a CNN. Left the original CNN (MaskRCNN) and different (2D and 3D) occlusion reasoning approaches improve the detection ([Reddy et al., 2019]).

More recent work using 3D information for occlusion reasoning has been introduced. Hsiao et al. argue that having 3D data provides richer information of the world, such as depth discontinuities and object size. [Pepikj et al., 2013] train multiple occlusion detectors on mined 3D annotated urban street scenes that contain distinctive, reoccurring occlusion patterns. [Wang et al., 2013] use RGB-D information and an extended Hough voting to include object location and its visibility pattern. [Radwan et al., 2013] addresses precisely the problem of self-occlusion in the context of human pose estimation and adds an inference step to handle self-occlusion to an off-the-shelf body pose detector to increase its performance under self-occlusion. The solution leverages prior knowledge about the kinematics and orientations of the human pose to deal with self-occluding body parts.

Lastly, convolutional neural networks have shown promising results when it comes to different visual tasks like object classification, recognition, segmentation and 3D pose estimation. However, occlusion and, as will be shown in this work, self-occlusion pose significant challenges. [Reddy et al., 2019] introduce a framework to predict 2D and 3D locations of occluded key points for objects to mitigate the effect of occlusion on the performance. Evaluated on CAD data and a large image set of vehicles at busy city intersections, the approach increases the localization accuracy of MaskRCNN by about 10%. A self-occlusion example can be seen in Figure 5. [Li et al., 2019] uses deep supervision to fine-grain image classification. In their approach, they simulate challenging occlusion configurations between objects to enable reliable data-driven

occlusion reasoning. Occlusion is modelled by rendering multiple object configurations and extracting the visibility level of the object of interest. With the work of [Kortylewski et al., 2020]) a convolutional neural network is combined with the idea of part-based models. The authors introduce CompositionalNets. It is proposed to replace the fully-connected classification layer with a differentiable compositional model. The idea of CompositionalNets is to decompose images into objects and context, and then decompose objects into parts and objects' pose. Using various CNN backbone shows that the approach can learn features that are invariant to occlusion and discard occluders during classification, hence increasing performance, especially under occlusion. However, a trade-off is pointed out that a good occluder localization lowers classification performance because classification benefits from features that are invariant to occlusion, where, on the other hand, occluder localization requires a different type of features. Namely, ones that sensitive to occlusion. It is pointed out that it is essential to resolve this trade-off with new types of models.

3. Object Definitions

In this Section, we will talk about the creation of the objects, as well as their characterization.

With *TEOS*, we present in total 48 objects, split into two sets; L_1 and L_2 . The idea of having two sets is to support the different needs of research. L_1 consists of 36 objects in 18 complexity levels, hence tailored towards research exploring the effect of finely grained complexity changes. L_2 , on the other side, is made up of 12 objects in three complexity levels based on L_1 , so made up of complexity groups.

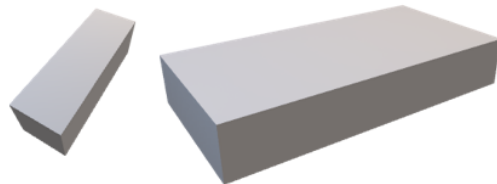


Figure 6. The building blocks used to create the objects of *TEOS*; cuboid (left) and base (right).

In a number of empirical studies, we have studied the relationship between the number of elements per object and classification accuracy. The human performance of classification L_1 objects is reliable (accuracy of $> 98\%$) for objects with up to seven elements. The classification gets uncertainty (89%) with objects consisting of around ten elements. Finally, the classification gets challenging (57%) with objects made of around 18 elements.

Based on these findings, we have created the L_2 set with three complexity levels; easy with seven elements, medium

with ten elements, and hard with 18 elements. For each complexity level, we have constructed three more objects with the same amount of elements but changing the orientation of one of the elements to have four distinct objects for each level. We will now continue to explain the elements used to assemble the objects and describe the objects' typical characteristics.

All objects consist of the following two elements:

- One 20mm x 60mm x 120mm base (Figure 6 right)
- n 20mm x 20mm x 60mm cuboids (Figure 6 left)



Figure 7. Possible connection points of cuboids on the base.

The complexity of an object is simply calculated as

$$compl = n + 1 \tag{1}$$

Where n is the number of cuboids used.

The base has five connection points for cuboids to be attached to. All cuboids are only attached upright, sitting flush with the bottom of the base. This also makes it simple to define a coordinate system. See Figure 8 for an illustration.

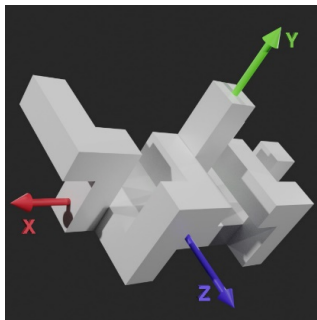


Figure 8. Illustration of the common coordinate system of the objects.

All objects share the same coordinate system, which is crucial for any research that looks at the effect of the orientational difference of 3D objects. The coordinate system

is defined as depicted in Figure 8; the Y-Axis is running orthogonal out of the base, the X-Axis running through the base from its center of gravity towards the end with three cuboids connectors, and the Z-Axis runs orthogonal to the Y- and X-Axis with the positive direction through the side of the base with two cuboid connections.

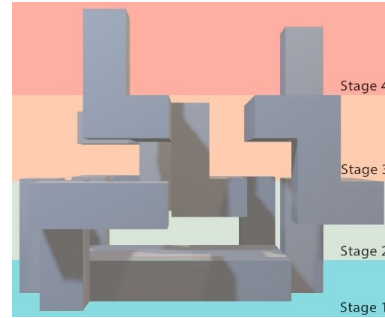


Figure 9. Stage-wise characterization of the objects. Another form of expressing the complexity of the object.

Building up the objects, a cuboid has eight connectors at which another cuboid can be attached. Consecutive cuboids are always orthogonal and never aligned in their direction, which is one of the differences to the Sheppard and Metzler objects. Furthermore, cuboids never intersect or touch neighbouring cuboids, hence avoiding geometrical loops. Creating the objects for L_1 , we focused on making the complexity comparable by consecutively adding one cuboid per complexity level.

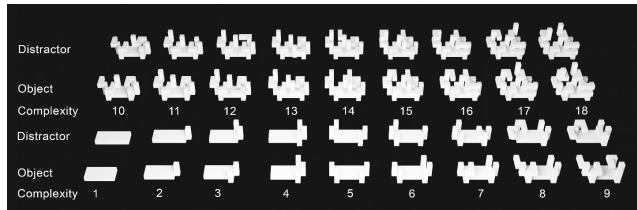


Figure 10. Illustration of L_1 with all 36 objects.

The objects can also be characterized in four stages of height. Each stage adds one perpendicular cuboid. For *TEOS*, four height-stages were introduced. Consequently, the number of height-stages presents another way of expressing the complexity of an object. An illustration of the different stages is given in Figure 9.

Lastly, having the objects characterized, we present the L_1 and L_2 object sets. The L_1 objects can be seen in Figure 10, and consist of 36 objects split into 18 complexity levels. There is a distractor object of the same complexity for each object that differs only in one small detail; one of the items is oriented differently. The introduction of the distractor objects is intended to support research in visual recognition,

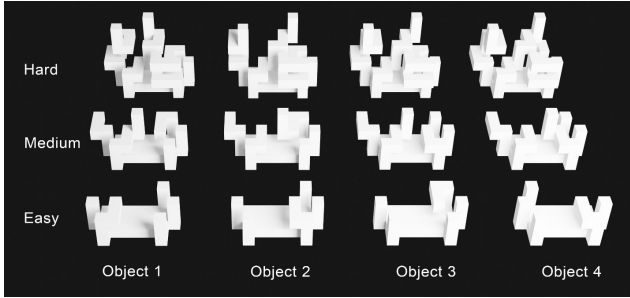


Figure 11. Illustration of L_2 with all 12 objects, split into three different complexity levels.

where merely counting the number of elements would reveal the object class.

On the other side, the L_2 set of objects is designed with less variation in complexity but more variation within a complexity. Twelve objects are evenly split into three complexity levels. To stick with the analogy of the distractors of the L_1 set, each complexity level of L_2 has three distractors; the same amount of elements but slight changes in assembling them. As described in the introduction of this Section, we chose the complexity levels based on empirical studies of visual recognition tasks. The L_2 objects can be seen in Figure 11.

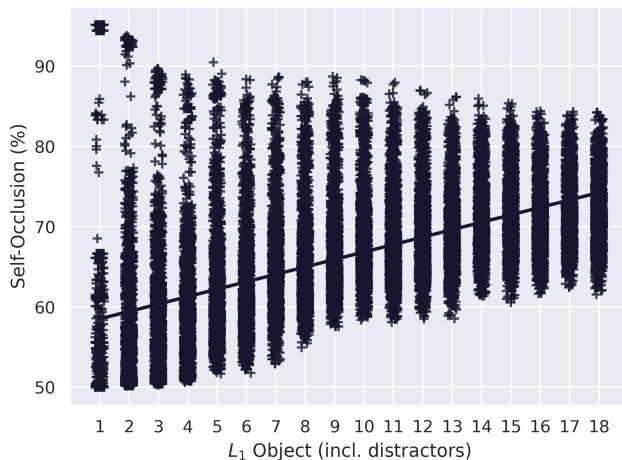


Figure 12. Illustration of the amount of average self-occlusion per object of L_1 .

An emphasis in designing these datasets was put on the ability to use them for self-occlusion studies. To accomplish this, all objects are built around a common coordinate system, share the same base and progressively add elements to increase the complexity and level of self-occlusion. Figure 12 shows how an increase of complexity of the L_1 dataset also increases the average amount of self-occlusion among all viewpoints. However, worth noting, with an increasing amount of complexity, the self-occlusion distribu-

tion per class decreases. Further information about our self-occlusion measure will be explained in Section 5.

4. Dataset Acquisition

TEOS is a dataset that is designed to be used in the virtual as well as the real world. For the former, one can use the rendered images and provided 3D Models (.STL file). For the latter, the objects are designed to be printable with a 3D printer. For this, we have prepared the 3D Models to be readable by many 3D printing slicing software. However, in this Section we want to focus on the generation of the rendered dataset images for which we have used Blender ([Blender, 2020]), a free and open-source 3D computer graphics software toolset. For *TEOS*, each object was rendered from 768 views – Totalling 36,864 images. To achieve realistic renderings of the objects, we used the Cycles Path Tracing rendering engine, created a white, smooth, plastic imitating material, set six light sources in the rendering scene and used 4096 paths to trace each pixel in the final rendering.

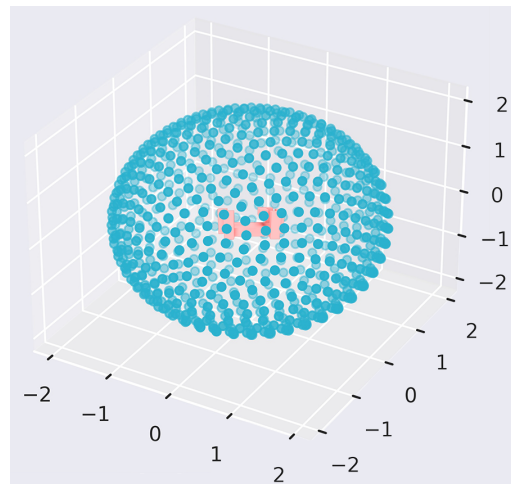


Figure 13. Illustration of viewpoints used to render each object of L_1 and L_2 . Views are evenly distributed on a sphere around an object (blue points) and point towards the object (light red). In total 768 views are taken.

Each object is rendered from the same set of views. To determine the views, we used the Fibonacci lattice ([Stanley, 1988]) approach. This approach allows distributing points on a sphere uniformly. Other approaches, for example, using radial distance, polar angle and azimuthal angle, will result in an unevenly sampled sphere; dense on the poles and sparse closer to the equator. Figure 13 illustrates the chosen views to generate the dataset. Each blue-coloured point represents a location where the camera is placed and oriented to the center where the object (red) is. We chose a sphere radius of two such that the object is

view-filling but not cropped in any view. Further, as it is sometimes practiced in the machine learning community ([Everingham et al., 2010, Lin et al., 2014, Matthey et al., 2017, Kabra et al., 2019]), we also provide the object mask and renderings with a dark and bright background for data augmentation purposes. The annotation file contains the object-type, view-id, bounding box information, object and camera positions and orientations, and object dimensions.

5. Self-Occlusion Measure

It seems evident that if we see less of an object, it is harder to classify it. Regions of the object that are occluded to us might hold distinct features to tell object X apart from object Y . In other words, occlusion for visual classification plays an important role. However, it is not only dependent on the view but also on the object. Let us take, for example, a sphere. No matter from which angle we look at it, we always observe 50% of it. On the contrary, for a complex polygonal shape, this cannot be answered as quickly as it is dependent on its geometry.

[Gay-Bellile et al., 2010] distinguishes two kinds of occlusions; “external occlusion” and “self-occlusion.” “External occlusion” is caused by an object entering the space between the camera and the object of interest and “self-occlusion” which describes the occlusion caused by the object of interest to itself. For *TEOS*, we are interested in the latter, as we always have one object in the scene. To our knowledge, no standard self-occlusion measure is used for computational approaches; therefore, we aim to specify our own intuitive measure as:

$$SO_{c_i} = \frac{A_{\phi}^{c_i}}{A_{\sigma}} \tag{2}$$

Where A_{ϕ} is defined as the occluded (not visible) surface area of the object and A_{σ} stands for the total surface area of the object.

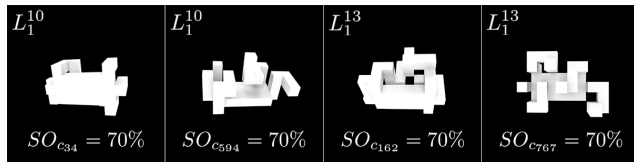


Figure 14. Examples of different objects (Object 10 and 13 of L_1) and poses causing the same amount of occlusion but different appearances.

An object might have different views from which it causes the same amount of self-occlusion, resulting in perhaps a considerably different appearance. Figure 14 shows an example of two objects from two different views with the same amount of occlusion. Therefore, we also consider the

camera’s point of view with c_i as the camera pose. Here, c_i is defined as the camera position $c_i = (x_i, y_i, z_i)$. Therefore, we also consider the camera’s point of view with c_i as the camera pose. Here, c_i is defined as the camera position $c_i = (x_i, y_i, z_i)$ and computed based on the Fibonacci lattice approach (see Figure 13). The camera orientation is automatically set such that the object is in the centre of the viewpoint.

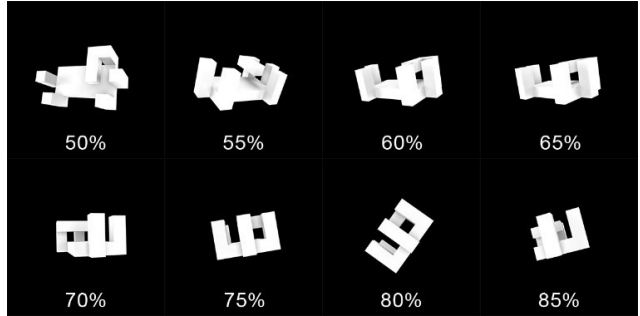


Figure 15. Examples of object viewpoints and their corresponding SO_{c_i} .

For evaluation purposes, we also define a function that maps a camera position (c_i) onto one of the eight regions of the octahedral viewing-sphere placed at the centre of an object. Figure 16 illustrates a mapping example for two camera-positions.

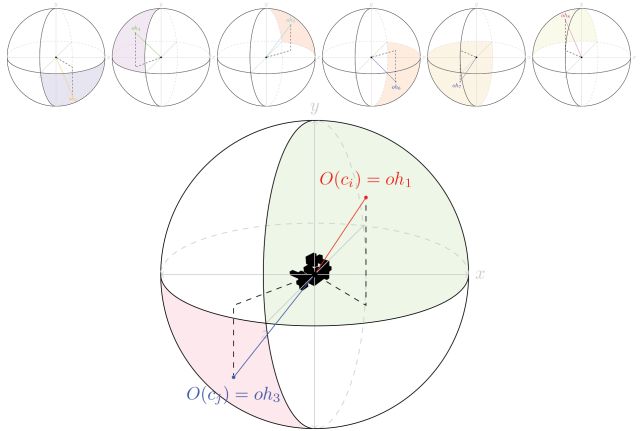


Figure 16. Visualization of the octahedron based projection used to map camera positions. Bottom: two example camera poses (c_i and c_j) mapped to oh_1 and oh_3 .

We represented the viewing sphere around an object as a spherically tiled octahedron, resulting in eight uniformly distributed triangles. To map a viewpoint c_i to a tile, we perform a determinant check to see in which tile a given camera pose c_i is located.

In our rendered data set, the self-occlusion was calculated by using the following steps:

1. Iterates over all faces of the object with valid normals and calculate the (A_σ)
2. Subdivide the objects into many thousand elements
3. Position the camera at a given location and pointing it at the object (see Figure 13)
4. Select all vertices that are visible through the camera view-port
5. Divide the object into two objects: visible and not-visible
6. Iterate over all faces of the not-visible object with valid normals and calculate (A_ϕ)
7. Lastly, calculate Self-Occlusion (Equation 2)

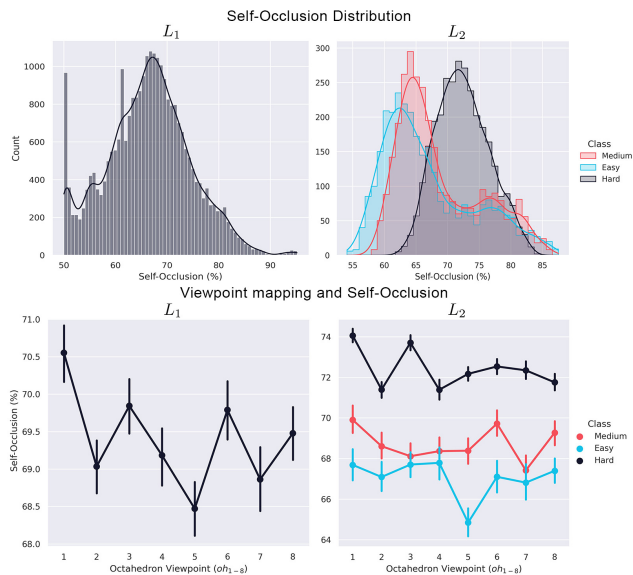


Figure 17. Illustration of the self-occlusion distribution for L_1 and L_2 (top), as well as the distributional relation between viewpoint mapping and self-occlusion for L_1 and L_2 (bottom).

Figure 15 shows eight examples of the same object (object-7) from different viewing angles and sorted based on their amount of self-occlusion. As can be seen in the illustration, a single object can cast many different appearances based on the viewing angle and a significant change in the amount of what is observable of it.

Figure 17 illustrates the self-occlusion distribution for L_1 and L_2 (top) and the distributional relation between viewpoint mapping and self-occlusion for L_1 and L_2 (bottom). Self-Occlusion for L_1 ranges from 49.99% to 95.16% with a mean at around 68% and L_2 from 54.08% to 87.5% with a mean at 61% (Easy), 63% (Medium), and 71% (Hard). The lower half of the Figure shows that different octahedron

viewpoints result in varying amounts of self-occlusion. For both L_1 and L_2 , a sweet-spot with the least self-occlusion is at oh_5 , presumably resulting in the best classification result.

6. Baseline Evaluation

In this Section, we discuss how well state-of-the-art classification approaches perform on *TEOS*. We have chosen five deep learning models with different properties, carefully trained and evaluated them on *TEOS*.

6.1. Model-Selection

We have chosen Inception-V3([Szegedy et al., 2016]), MobileNet-V2 ([Sandler et al., 2018]), ResNet-V2 ([He et al., 2016]), VGG16 ([Simonyan and Zisserman, 2014]) and EfficientNet ([Tan and Le, 2019]) as reference networks for *TEOS*. Their trained version of *TEOS* will be made publicly available. Table 1 shows more details about the networks in ascending order of their parameter count.

Table 1. High-Level CNN Characteristics

CNN	Layers	Parameters (mil.)
MobileNet-V2	53	3.4
Inception-V3	48	24
ResNet-V2	152	58.4
EfficientNet-B7	813	66
VGG16	152	138

With *TEOS*'s unique characteristics, it is not trivial to tell which CNN architecture will perform better or worse. Therefore, we chose networks with varying numbers of parameters and different numbers of layers.

6.2. Training-Parameter

Besides the architecture of CNNs, a crucial element is the choice of training-parameters and so-called hyperparameters. In our case, we have looked at the input size, input noise, dropout rate, learning rate, optimization algorithm and lastly, the difference between learning from scratch and fine-tuning the networks. Hyperparameters such as input noise, dropout rate, learning rate were determined using the hyperparameter optimizer Hyperband by [Li et al., 2017]. The remaining parameters were empirically determined. Table 2 presents the parameters used to establish the baseline of *TEOS*.

6.3. Training Data Preparation

To prepare the data for training, we chose a 20% validation split and augmented the remaining 80% with standard data augmentation techniques ([Shorten and Khoshgoftaar, 2019]). See Table 3:

Table 2. Chosen Training Parameters

Parameter	Value
Input Size	224 x 224 – 800 x 800 (dependent on CNN)
Input Noise	Gaussian Noise of 0.1
Drop Rate	20%
Learning Rate	1e-5
Optimizer	Adam Optimization
Learning Method	Fine Tuning

Table 3. Parameters for Data Augmentation

Data Augmentation Technique	Value
Rotation	0-40 degrees
Width Shift	0-20%
Height Shift	0-20%
Zoom	0-20%

6.4. Classification Results

Our results show that MobileNet-V2 performed best across L_1 and L_2 . Specifically, for L_1 , it achieved a top-1 accuracy of 17.25% and 10.83% on the L_2 data set. See Figure 18 for the classification accuracies of all networks. It seems that MobileNet-V2 is the only network that was able to learn some aspects of *TEOS*, performing with a large (L_1) or small (L_2) margin above chance, whereas all other networks perform at around chance. This, perhaps, has something to do with the relatively homogeneous appearance of *TEOS*, not allowing the more complex CNNs to learn from. However, this needs to be investigated further in the future.

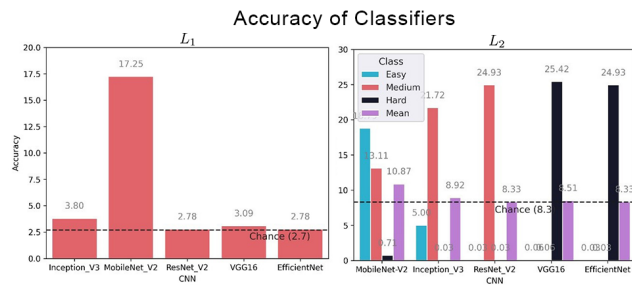


Figure 18. Evaluation results on L_1 (left) and L_2 (right) for five different CNNs and their accuracy across the entire datasets.

Generally, L_2 is more challenging to learn for CNNs than L_1 . Even the best performing CNN is only 2.53% above chance, where this margin for L_1 was at about 14.5%. This is explainable with the high intra-class similarity of L_2 – objects of one class look very similar to each other and only vary in one small detail, which might be only observable from certain viewpoints, hence will be confused with each other.

The L_1 dataset, on the other side, has a low inter-class similarity – the appearance of objects varies between classes.

A closer look at the results of L_2 reveals that more extensive networks (VGG16 and EfficientNet-B7) were able to learn objects of class “Hard” of L_2 ; however, they could not learn “Medium” and “Easy” Objects. The smaller networks, on the other hand (MobileNet-V2 and Inception-V3), were able to learn “Easy” and “Medium” objects but not “Hard.” Except for MobileNet-V2, all networks have profound problems to learn the “Easy” Objects. See Figure 18 for details.

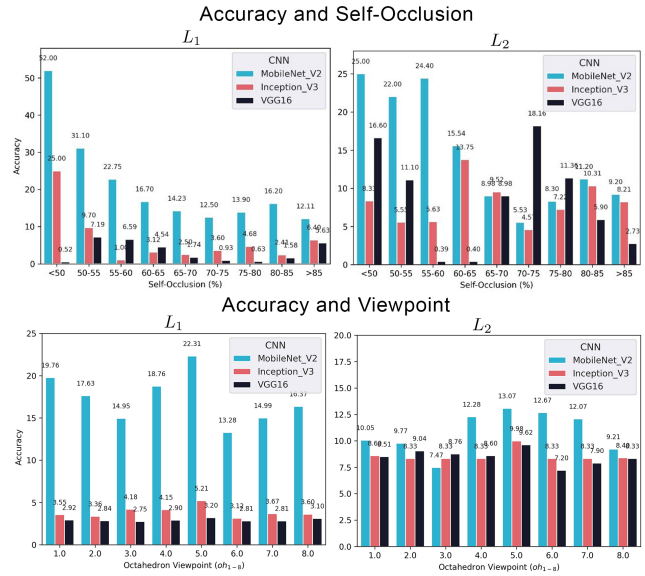


Figure 19. Evaluation results on L_1 and L_2 for the three top-performing CNNs. Top: Accuracy across the entire datasets with respect to self-occlusion. Bottom: Accuracy and how it is affected by the chosen viewpoint.

Regarding the connection between classification accuracy and amount of self-occlusion, it can be generally said that the classification accuracy goes down if self-occlusion increases. We have chosen the three best-performing CNNs to analyze this connection and grouped L_1 and L_2 from 50% to 85% self-occlusion in 5% intervals. $< 50\%$ captures all viewpoints with a self-occlusion of less than 50%. $> 85\%$ includes all images with more than 85%. Furthermore, we also investigated the connection between the viewpoint mapped to an octahedral viewing-sphere and accuracy. As can be seen in the example of L_1 and MobileNet-V2, the viewpoint does play a vital role and can result in an increase of accuracy performance by $13.28 \leftrightarrow 22.31 = 67.99\%$. Across L_1 and L_2 the octahedral viewpoint resulting in the best performance was oh_5 . This can be explained with that all objects share a common coordinate system and shows once more that the viewpoint matters and, even more, that an *ideal viewpoint* can exist. See Figure 19 for details.

Further, even though the CNNs are trained and validated on the entire data set, their best performance can be seen

at lower self-occlusion rates, which shows the vital role of self-occlusion for object classification performance.

7. Conclusion and Future Directions

In this work, we have presented a novel 3D blocks world dataset that focuses on the geometric shape of 3D objects and their omnipresent challenge of self-occlusion. We have created two data sets, L_1 and L_2 , including hundreds of high-resolution, realistic renderings from known camera angles. Each data set also comes with rich annotations. Further, we have presented a simple but precise measure of self-occlusion and were able to show how self-occlusion challenges the classification accuracy of state-of-the-art CNNs and the viewpoint can benefit the classification.

Lastly, in our baseline evaluation, we have presented that CNNs are unable to learn *TEOS*, leaving much room for future work improvements.

We hope to have pathed a way to explore the relationship between object classification, viewpoint, and self-occlusion with this work. Specifically, we hope that *TEOS* is useful for research in the realm of active vision – to plan and reason for the next-best-view seems to be crucial to increase object classification performance.

8. Acknowledgements

This research was supported by grants to the senior author (JKT) from the following sources: Air Force Office of Scientific Research USA (FA9550-18-1-0054), The Canada Research Chairs Program (950-231659) and Natural Sciences and Engineering Research Council of Canada (RGPIN-2016-05352). The funders had no role in study design, data collection and analysis, decision to publish, or preparation of the manuscript.

References

- [Andreopoulos and Tsotsos, 2013] Andreopoulos, A. and Tsotsos, J. K. (2013). 50 Years of object recognition: Directions forward. *Computer Vision and Image Understanding*, 117(8):827–891.
- [Blender, 2020] Blender (2020). *Blender - a 3D modelling and rendering package*. Blender Foundation, Stichting Blender Foundation, Amsterdam.
- [Brachmann et al., 2014] Brachmann, E., Krull, A., Michel, F., Gumhold, S., Shotton, J., and Rother, C. (2014). Learning 6D object pose estimation using 3D object coordinates. *Lecture Notes in Computer Science (including subseries Lecture Notes in Artificial Intelligence and Lecture Notes in Bioinformatics)*, 8690 LNCS(PART 2):536–551.
- [Carroll and Others, 1993] Carroll, J. B. and Others (1993). *Human cognitive abilities: A survey of factor-analytic studies*. Cambridge University Press.
- [Clowes, 1971] Clowes, M. B. (1971). On seeing things. *Artificial intelligence*, 2(1):79–116.
- [Dollár et al., 2012] Dollár, P., Wojek, C., Schiele, B., and Perona, P. (2012). Pedestrian detection: An evaluation of the state of the art. *IEEE Transactions on Pattern Analysis and Machine Intelligence*, 34(4):743–761.
- [Ess et al., 2009] Ess, A., Schindler, K., Leibe, B., and Van Gool, L. (2009). Improved multi-person tracking with active occlusion handling. In *ICRA Workshop on People Detection and Tracking*, volume 2. Citeseer.
- [Everingham et al., 2010] Everingham, M., Van Gool, L., Williams, C. K. I., Winn, J., and Zisserman, A. (2010). The pascal visual object classes (VOC) challenge. *International Journal of Computer Vision*, 88(2):303–338.
- [Gay-Bellile et al., 2010] Gay-Bellile, V., Bartoli, A., and Sayd, P. (2010). Direct estimation of nonrigid registrations with image-based self-occlusion reasoning. *IEEE Transactions on Pattern Analysis and Machine Intelligence*, 32(1):87–104.
- [Girshick et al., 2011] Girshick, R., Felzenszwalb, P., and McAllester, D. (2011). Object detection with grammar models. *Advances in neural information processing systems*, 24:442–450.
- [He et al., 2015] He, K., Zhang, X., Ren, S., and Sun, J. (2015). Delving Deep into Rectifiers: Surpassing Human-Level Performance on ImageNet Classification. In *Proceedings of the IEEE international conference on computer vision*.
- [He et al., 2016] He, K., Zhang, X., Ren, S., and Sun, J. (2016). Identity mappings in deep residual networks. In *European conference on computer vision*, pages 630–645. Springer.
- [Hinterstoisser et al., 2013] Hinterstoisser, S., Lepetit, V., Ilic, S., Holzer, S., Bradski, G., Konolige, K., and Navab, N. (2013). Model based training, detection and pose estimation of textureless 3D objects in heavily cluttered scenes. In *Lecture Notes in Computer Science (including subseries Lecture Notes in Artificial Intelligence and Lecture Notes in Bioinformatics)*, volume 7724 LNCS, pages 548–562.
- [Hsiao et al., 2010] Hsiao, E., Collet, A., and Hebert, M. (2010). Making specific features less discriminative to improve point-based 3D object recognition. *Proceedings of the IEEE Computer Society Conference on Computer Vision and Pattern Recognition*, pages 2653–2660.
- [Hsiao and Hebert, 2014] Hsiao, E. and Hebert, M. (2014). Occlusion reasoning for object detection under arbitrary viewpoint. *IEEE Transactions on Pattern Analysis and Machine Intelligence*, 36(9):1803–1815.
- [Huffman, 1971] Huffman, D. A. (1971). Impossible object as nonsense sentences. *Machine intelligence*, 6:295–324.
- [Kabra et al., 2019] Kabra, R., Burgess, C., Matthey, L., Kaufman, R. L., Greff, K., Reynolds, M., and Lerchner, A. (2019). Multi-Object Datasets. <https://github.com/deepmind/multi-object-datasets/>.
- [Kirosis and Papadimitriou, 1988] Kirosis, L. M. and Papadimitriou, C. H. (1988). The complexity of recognizing polyhedral scenes. *Journal of Computer and System Sciences*, 37(1):14–38.

- [Koporec and Pers, 2019] Koporec, G. and Pers, J. (2019). Deep learning performance in the presence of significant occlusions - An intelligent household refrigerator case. *Proceedings - 2019 International Conference on Computer Vision Workshop, IC-CVW 2019*, pages 2532–2540.
- [Kortylewski et al., 2020] Kortylewski, A., Liu, Q., Wang, A., Sun, Y., and Yuille, A. (2020). Compositional Convolutional Neural Networks: A Robust and Interpretable Model for Object Recognition Under Occlusion. *International Journal of Computer Vision*, (Economist 2017).
- [Kuznetsova et al., 2020] Kuznetsova, A., Rom, H., Alldrin, N., Uijlings, J., Krasin, I., Pont-Tuset, J., Kamali, S., Popov, S., Mallocci, M., Kolesnikov, A., Duerig, T., and Ferrari, V. (2020). The Open Images Dataset V4: Unified Image Classification, Object Detection, and Visual Relationship Detection at Scale. *International Journal of Computer Vision*, 128(7):1956–1981.
- [Li et al., 2019] Li, C., Zia, M. Z., Tran, Q. H., Yu, X., Hager, G. D., and Chandraker, M. (2019). Deep Supervision with Intermediate Concepts. *IEEE Transactions on Pattern Analysis and Machine Intelligence*, 41(8):1828–1843.
- [Li et al., 2017] Li, L., Jamieson, K., DeSalvo, G., Rostamizadeh, A., and Talwalkar, A. (2017). Hyperband: A novel bandit-based approach to hyperparameter optimization. *The Journal of Machine Learning Research*, 18(1):6765–6816.
- [Lin et al., 2014] Lin, T. Y., Maire, M., Belongie, S., Hays, J., Perona, P., Ramanan, D., Dollár, P., and Zitnick, C. L. (2014). Microsoft COCO: Common objects in context. *Lecture Notes in Computer Science (including subseries Lecture Notes in Artificial Intelligence and Lecture Notes in Bioinformatics)*, 8693 LNCS(PART 5):740–755.
- [Matthey et al., 2017] Matthey, L., Higgins, I., Hassabis, D., and Lerchner, A. (2017). dSprites: Disentanglement testing Sprites dataset. <https://github.com/deepmind/dsprites-dataset/>.
- [Meger et al., 2011] Meger, D., Wojek, C., Little, J. J., and Schiele, B. (2011). Explicit Occlusion Reasoning for 3D Object Detection. In *BMVC*, pages 1–11. Citeseer.
- [Ouyang and Wang, 2012] Ouyang, W. and Wang, X. (2012). A discriminative deep model for pedestrian detection with occlusion handling. *Proceedings of the IEEE Computer Society Conference on Computer Vision and Pattern Recognition*, pages 3258–3265.
- [Parodi et al., 1998] Parodi, P., Lancewicki, R., Vjih, A., and Tsotsos, J. K. (1998). Empirically-derived estimates of the complexity of labeling line drawings of polyhedral scenes. *Artificial Intelligence*, 105:47–75.
- [Pepikj et al., 2013] Pepikj, B., Stark, M., Gehler, P., and Schiele, B. (2013). Occlusion patterns for object class detection. In *Proceedings of the IEEE Conference on Computer Vision and Pattern Recognition*, pages 3286–3293.
- [Radwan et al., 2013] Radwan, I., Dhall, A., and Goecke, R. (2013). Monocular image 3D human pose estimation under self-occlusion. *Proceedings of the IEEE International Conference on Computer Vision*, pages 1888–1895.
- [Reddy et al., 2019] Reddy, N. D., Vo, M., and Narasimhan, S. G. (2019). Occlusion-net: 2d/3d occluded keypoint localization using graph networks. In *Proceedings of the IEEE Conference on Computer Vision and Pattern Recognition*, pages 7326–7335.
- [Roberts, 1965] Roberts, L. G. (1965). *Machine perception of three-dimensional solids*. MIT Press, Cambridge, MA.
- [Russakovsky et al., 2015] Russakovsky, O., Deng, J., Su, H., Krause, J., Satheesh, S., Ma, S., Huang, Z., Karpathy, A., Khosla, A., Bernstein, M., Berg, A. C., and Fei-Fei, L. (2015). ImageNet Large Scale Visual Recognition Challenge. *International Journal of Computer Vision (IJCV)*, 115(3):211–252.
- [Sandler et al., 2018] Sandler, M., Howard, A., Zhu, M., Zhmoginov, A., and Chen, L.-C. (2018). Mobilenetv2: Inverted residuals and linear bottlenecks. In *Proceedings of the IEEE conference on computer vision and pattern recognition*, pages 4510–4520.
- [Shepard and Metzler, 1971] Shepard, R. N. and Metzler, J. (1971). Mental Rotation of Three-Dimensional Objects. 171(3972):701–703.
- [Shorten and Khoshgoftaar, 2019] Shorten, C. and Khoshgoftaar, T. M. (2019). A survey on Image Data Augmentation for Deep Learning. *Journal of Big Data*, 6(1).
- [Shu et al., 2012] Shu, G., Dehghan, A., Oreifej, O., Hand, E., and Shah, M. (2012). Part-based multiple-person tracking with partial occlusion handling. In *2012 IEEE Conference on Computer Vision and Pattern Recognition*, pages 1815–1821. IEEE.
- [Simonyan and Zisserman, 2014] Simonyan, K. and Zisserman, A. (2014). Very deep convolutional networks for large-scale image recognition. *arXiv preprint arXiv:1409.1556*.
- [Slaney and Thiébaux, 2001] Slaney, J. and Thiébaux, S. (2001). *Blocks World revisited*, volume 125.
- [Solbach et al., 2018] Solbach, M. D., Volland, S., Edmonds, J., and Tsotsos, J. K. (2018). Random polyhedral scenes: An image generator for active vision system experiments.
- [Stanley, 1988] Stanley, R. P. (1988). Differential posets. *Journal of the American Mathematical Society*, 1(4):919–961.
- [Szegedy et al., 2016] Szegedy, C., Vanhoucke, V., Ioffe, S., Shlens, J., and Wojna, Z. (2016). Rethinking the Inception Architecture for Computer Vision. In *Proceedings of the IEEE Conference on Computer Vision and Pattern Recognition (CVPR)*.
- [Tan and Le, 2019] Tan, M. and Le, Q. V. (2019). Efficientnet: Rethinking model scaling for convolutional neural networks. *arXiv preprint arXiv:1905.11946*.
- [Tsotsos et al., 2005] Tsotsos, J. K., Liu, Y., Martinez-Trujillo, J. C., Pomplun, M., Simine, E., and Zhou, K. (2005). Attending to visual motion. *Computer Vision and Image Understanding*, 100(1-2 SPEC. ISS.):3–40.
- [Vedaldi and Zisserman, 2009] Vedaldi, A. and Zisserman, A. (2009). Structured output regression for detection with partial truncation. *Advances in neural information processing systems*, 22:1928–1936.

- [Wang et al., 2013] Wang, T., He, X., and Barnes, N. (2013). Learning structured hough voting for joint object detection and occlusion reasoning. In *Proceedings of the IEEE Conference on Computer Vision and Pattern Recognition*, pages 1790–1797.
- [Wang et al., 2009] Wang, X., Han, T. X., and Yan, S. (2009). An HOG-LBP human detector with partial occlusion handling. In *2009 IEEE 12th international conference on computer vision*, pages 32–39. IEEE.
- [Wu and Nevatia, 2009] Wu, B. and Nevatia, R. (2009). Detection and segmentation of multiple, partially occluded objects by grouping, merging, assigning part detection responses. *International journal of computer vision*, 82(2):185–204.
- [Xing et al., 2009] Xing, J., Ai, H., and Lao, S. (2009). Multi-object tracking through occlusions by local tracklets filtering and global tracklets association with detection responses. In *2009 IEEE Conference on Computer Vision and Pattern Recognition*, pages 1200–1207. IEEE.